Impact of Different Modeling Approaches in Field Focusing Predictions of Hyperthermia Cancer Therapy

R. Gaffoglio[1*], G. Vecchi[2], M. Righero[1], G. Giordanengo[1], M. Zucchi[2].

[1] Advanced Computing and Applications, LINKS Foundation, Torino, Italy
[2] Department of Electronics and Telecommunications, Politecnico di Torino, Torino, Italy
[*] Corresponding author: rossella.gaffoglio@linksfoundation.com

Abstract: The fundamental aim of an oncological hyperthermia treatment consists in heating the tumour region to a temperature of about 42/43 °C, while keeping the heat in the surrounding healthy tissues in a tolerable range. With the aid of the COMSOL Multiphysics® simulation software and the LiveLink™ for MATLAB® module, we reproduced a typical microwave applicator specifically designed for targeted heating of deep-seated head and neck (H&N) tumours, and we analyze how a SAR-based field optimization on the target volume could be implemented for different models of the neck region.

1. Introduction

The hyperthermia treatment (HT), i.e. an increase of the body tissues temperature to 39-43 °C caused by the exposure to non-ionizing electromagnetic radiation (like radiofrequency or microwaves), has been demonstrated to sensitize tumours to radiotherapy and chemotherapy (i.e. cancer therapies are more effective at the same dose), without adding toxicity [1]. The comparison in terms of clinical outcome between oncology patients treated with radiotherapy alone vs. thermo-radiotherapy (i.e. radiotherapy plus hyperthermia treatment) has demonstrated how HT provides significant benefits for different tumour sites, such as breast, cervix, head neck, rectum and urinary bladder [1]. Moreover, many chemotherapeutic agents exhibit synergism with HT [2]; indeed, hyperthermia improves the specific delivery of chemotherapy drugs to the target by means of different mechanisms, including an increase in the tumour oxygenation and the enhanced possibility of inflicting DNA damage and inhibition of repair.

One of the more critical aspects of a hyperthermia treatment is the constant need to accurately monitor the patient's internal temperature to ensure an optimal heating of the tumour while avoiding the presence of hot spots in the surrounding healthy regions, especially in thermosensitive tissues (like cerebrum, cerebellum, spinal cord, etc.).

To do this, the power supplies of the employed microwave applicator are properly adjusted optimizing the energy absorption rate (SAR) or the temperature increase in the tumour region by means of bio-electromagnetic solvers, where both the antenna system geometry and the segmented model of the patient's region of interest (ROI) are reproduced. In the clinical practice, suitable softwares offer complete 3D image segmentation and model generation solutions from CT and MRI scans of the patient, converting image data to Finite Element detailed models. However, outside of clinical practice, the numerical studies concerning the applicator design as well as the optimization techniques relative to the field focusing require the use of generic (not patient-specific) computational phantoms of the human body.

In the presented work, we reproduced a simplified version of an array applicator system [3,4], which is basically an array of patch antennas specifically designed to treat tumours in the head and neck (H&N) region. Then, using the LiveLink™ for MATLAB® module, we implemented a SAR-based optimization of the antenna feedings aimed at maximizing the deposited energy on the target region avoiding energy spots in the healthy tissues, showing the application of this procedure to different neck models designed with COMSOL Multiphysics®. The first model consists in a very simple representation of the human neck, where the vertebras, the spinal cord, the trachea as well as the neck shape are modeled by means of cylinders, while the tumour is represented by a sphere.
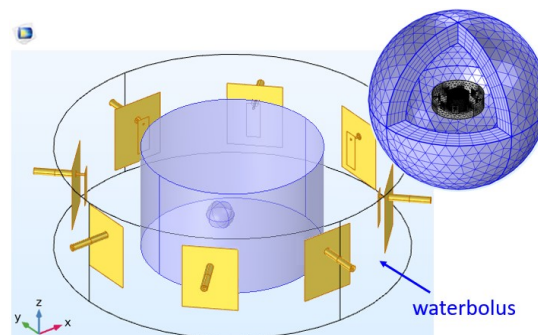

Figure 1. Geometry of the array applicator, the neck phantom and the waterbolus. The inset shows the surrounding air domain and PML layer.

Table 1. Volume density and dielectric properties of the considered tissues at f = 434 MHz [8].

Tissue type	ρ [kg/m³]	ε_r [-]	σ [S/m]
Skin (wet)	1109	0.681	49.4
Fat	911	0.082	11.6
Muscle	1090	0.805	56.9
Bone	1908	0.094	13.1
Spinal cord	1075	0.456	35.0
Internal air	1.13	0	1
Thyroid	1050	0.886	61.3
Tumour[9]	1050	0.890	59.0

Then, we implemented a more realistic neck phantom importing in COMSOL Multiphysics freely downloadable meshed human models [5]. Finally, we tried to reproduce the neck phantom characteristics through the definition of proper material functions interpolating a set of voxel data [6,7], as described in the last section.

2. H&N hyperthermia applicator

To perform HT on deep-seated tumours in the head and neck (H&N) region, the most common applicator is a circular or elliptical array of antennas matched to the patient's neck by means of a waterbolus filled with (demineralized) circulating water [3], having also the fundamental function to avoid the body surface overheating. Using the COMSOL Multiphysics software, we reproduced this applicator as a uniform circular array with N_T = 8 patch antennas properly matched at the operating frequency f = 434 MHz, and totally immersed in an external cylinder filled with demineralized water at a constant temperature T = 25 °C with dielectric properties ε_r = 78, σ = 0.04 S/m [4]. Using patch antennas with a water substrate not only enables a more efficient radiation into the waterbolus, but also considerably decreases the optimal size of the antennas [4]. The geometry of the simulated radiating system is reported in Fig. 1. As can be observed, both the antenna array and the waterbolus surround the neck phantom, and the whole system is inserted in a spherical air volume, wrapped by a spherical Perfectly Matched Layer (PML), created by means of an extrusion operation. The patch antennas have been modelled with infinitely thin Perfect Electric Conductor (PEC) layers and fed by means of Coaxial Lumped ports properly sized to ensure a characteristic impedance of 50 Ω.

2. SAR-based optimization

To maximize the energy deposition inside the tumour, reducing the risk of hot-spots in the surrounding healthy tissues, the relative powers and phases of each individual antenna can be optimized using different approaches. A possible strategy, clinically used nowadays for different applicators, is the so-called Hot spot SAR to Tumour SAR Quotient Particle Swarm Optimization (PSO), where the goal function to minimize is given by [10]:

$$HTQ(\boldsymbol{r}) = \frac{\langle SAR^H(\boldsymbol{r}) \rangle_{1\%}}{\langle SAR^T(\boldsymbol{r}) \rangle} \qquad (1)$$

where $< SAR^T >$ is the mean SAR in the target region, while $< SAR^H >_{1\%}$ is the hot spot SAR, defined as the average SAR in V1, which is the 1% of the healthy volume with the highest SAR.

To implement this SAR-based optimization the total electric field generated by the antenna array must be considered, i.e.:

$$\boldsymbol{E}_{tot}(\boldsymbol{r}) = \sum_{n=1}^{N_T} \tilde{v}_n \, \boldsymbol{e}_n(\boldsymbol{r}) \qquad (2)$$

where:

$$\tilde{v}_n = v_n \exp(i\varphi_n) \in \mathbb{C} \qquad (3)$$

are the complex feedings of the array elements, while $\boldsymbol{e}_n$ is the electric field generated by the nth antenna acting as standalone, i.e. when only the nth antenna is switched on with a standardized input signal (1 V, zero phase).

Using the LiveLink for MATLAB module, we generated a routine that runs N_T times our COMSOL model (only involving the RF module), feeding one antenna at a time. Then, at each step, the complex components of the electric field evaluated on the tumour and the healthy domains are separately stored in proper structure arrays. To control which domain is used for exporting the data, we added a selection sub-node to the data set, selecting the appropriate domain in this node (before running the data export). Using the stored electric field data, automatically saved thanks to the LiveLink for MATLAB module, we computed the SAR distribution in the tumour and in the surrounding
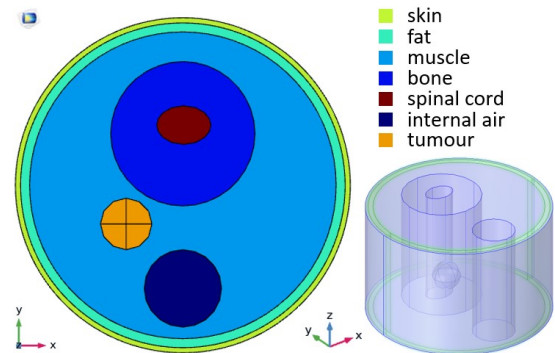

Figure 2. Middle top view (*left*) and side view (*right*) of the simplified neck model with all the considered tissues.
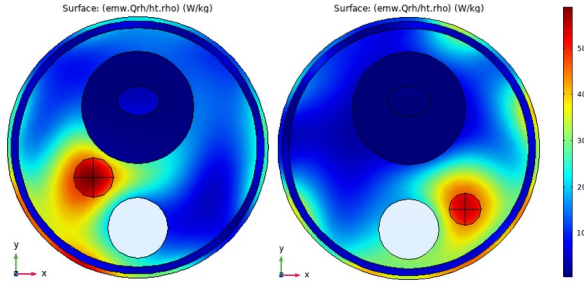
Figure 3. Middle top view of the SAR distribution in the simplified neck model for two different sites of the tumour, with radius 10 mm (*left*) and 8 mm (*right*).

healthy tissues, separately, by means of the following expression:

$$SAR(\boldsymbol{r}) = \frac{1}{2\rho(\boldsymbol{r})}\,\sigma(\boldsymbol{r})\,|\boldsymbol{E}_{tot}(\boldsymbol{r})|^2 \qquad (4)$$

where σ and ρ are the electrical conductivity and volume density in the neck model, varying according to the materials assigned to the different regions and provided by COMSOL through the Export node. Then, we implemented an objective function in MATLAB which takes in input the relative feedings of the antennas and evaluates the Hot spot SAR to Tumour SAR Quotient defined in (1) using the electric field data previously computed with COMSOL Multiphysics.

A Particle Swarm Optimization (PSO) aimed at minimizing the above-described goal function is finally computed in MATLAB, varying the $N_T = 8$ input phases between 0 and 2π, using a swarm size of 100 individuals and adding the MATLAB hybrid function '*fmincon*' to refine the optimization when the particle swarm terminates.

At the beginning, we decided to optimize only the relative phases of each individual antenna φ_n, by
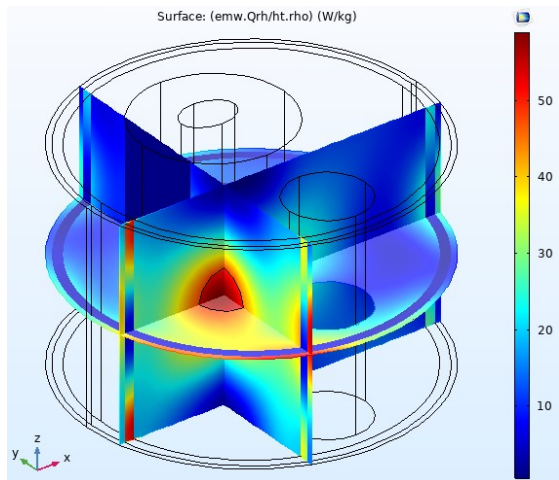

Figure 4. SAR distribution in the simplified neck model for the tumour configuration reported in the left picture of Fig. 3.
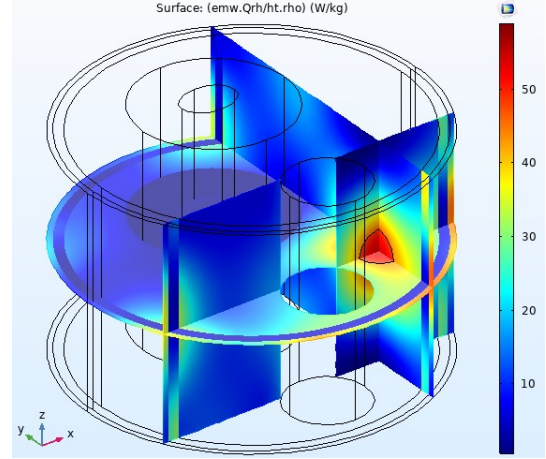

Figure 5. SAR distribution in the simplified neck model for the tumour configuration reported in the right picture of Fig. 3.

imposing $v_n = \sqrt{2RP_{in}/N_T}$ on each antenna, where $R = 50\ \Omega$ is the antenna resistance, while P_{in} is the total array input power.

3. Simplified neck model

As a first step, we realized a very simple representation of the human neck, modeled as a cylinder with radius $R_N = 65$ mm and height $H_N = 81$ mm. As shown in Fig. 2, the vertebras, the spinal cord and the laryngotracheal air canal are also modeled by means of cylinders, while the tumour is represented by a sphere. The IT'IS [8] electrical and thermal parameters have been properly assigned to the different tissues by creating different Material sub-nodes. Table 1 reports the volume densities and dielectric properties associated to the considered tissues at the operating frequency $f = 434$ MHz.

The SAR-based optimization described in Section 2 has been implemented for different locations and sizes of the tumour (see Fig. 3), providing each time an optimal set of antenna phases φ_n after about 100 iterations. Figures 4 and 5 show the obtained SAR distribution on three planes cutting the tumour along the canonical directions, for the two configurations reported in Fig. 3, respectively. As can be observed, the SAR is correctly focused all over the tumour volume. Some areas with high SAR are inevitably localized on the skin; however, these areas will not cause temperature spots, thanks to the waterbolus cooling function.

4. Realistic neck model

Crucial inputs for hyperthermia treatment planning are the 3D patient models incorporating the tumour and the surrounding healthy tissues, that need to be
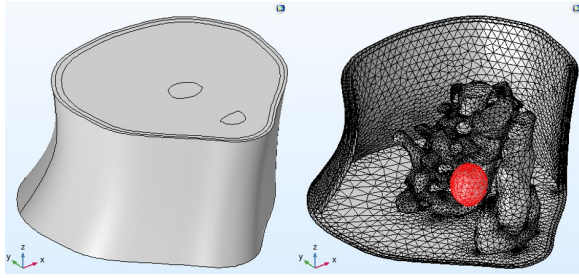
Figure 6. Geometry (*left*) and mesh (*right*) of the realistic neck model implemented in COMSOL Multiphysics.
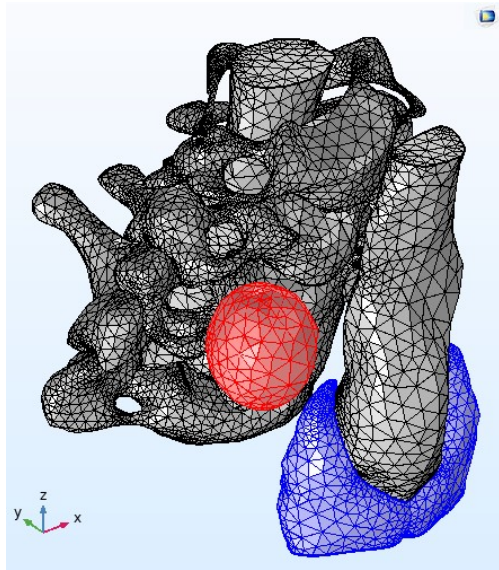

Figure 7. Mesh of the imported realistic elements. The tumour and the thyroid gland are highlighted.

Figure 8. Surface visualization of the SAR distribution in the realistic neck model, focused on the tumour site.

accurately segmented to properly capture the impact of strong dielectric and thermal properties gradients. Hence, to make our analyses closer to the clinical practice, we implemented a more realistic neck phantom importing in COMSOL Multiphysics the 3D mesh models of the vertebras (from C3 to C7), the spinal cord and the laryngotracheal canal provided by the Visible Human Project (VHP-Female Version 2.2 [5]).

Indeed, COMSOL Multiphysics supports the import of surface meshes from STL files, as described in [11]. Each STL file can be imported in COMSOL from the Geometry node to create a solid geometry object; as a result of the Import operation, a Mesh Part sequence is added under the Global Definitions - Mesh Parts node. The Mesh Part sequence becomes the source for the geometry import; then, some tools like the Joined Entities operation can be used to strongly improve the mesh-to-object conversion. Once the VHP STL files are imported in the model, and properly converted to 3D objects, they can be robustly meshed with COMSOL Multiphysics.
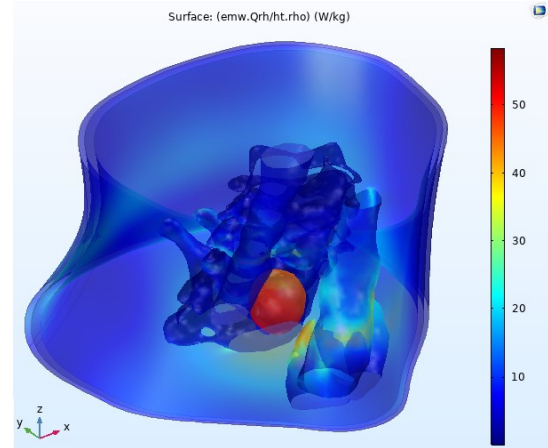
As shown in Figures 6 and 7, in this second neck phantom the tumour is modeled as a sphere of irregular shape, and the thyroid gland is also reproduced (starting from a freely downloadable CAD file). Then, using the several geometry operations, tools, and functionalities of COMSOL Multiphysics, we realized a more sinuous shape for the human neck (see Fig. 6), giving a more realistic look to the phantom.

The electric fields generated by each antenna acting as standalone were computed again for this new model with LiveLink for MATLAB, and the minimization of the objective function (1) by means of a Particle Swarm Optimization was performed. The resulting SAR distribution is reported in Figures 8 and 9. Although the Surface plot (Fig. 8) shows a good SAR focusing on the tumour, the visualization of the SAR distribution on the cut planes (Fig. 9) reveals a significant spread outside the target region.
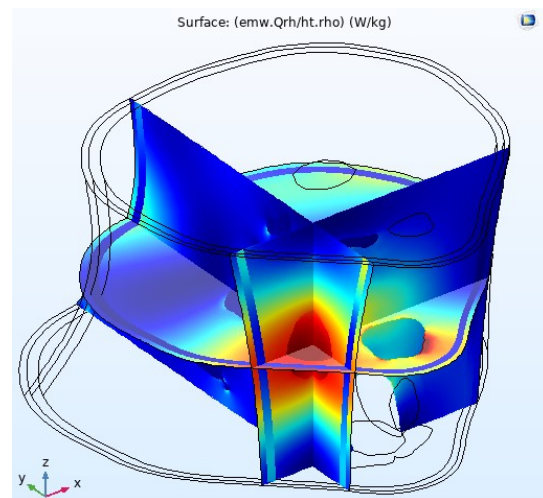

Figure 9. SAR distribution in the realistic neck model over three cut planes cutting the tumour along the canonical directions.
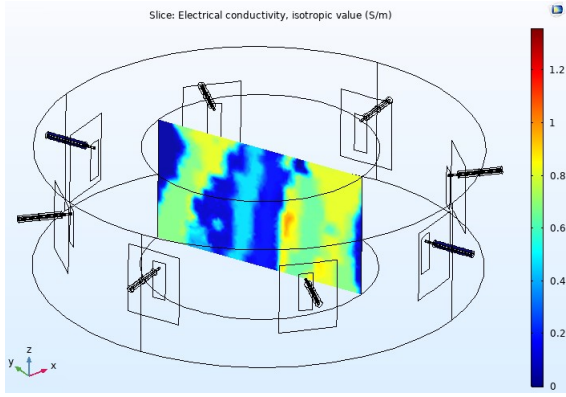
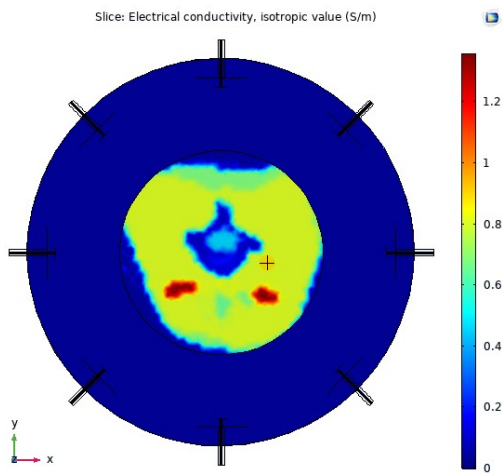**Figure 10.** Visualization of the electrical conductivity of the interpolated neck model, on the *yz* plane.

Figure 11. Electrical conductivity displayed on the *xy* plane cutting the model at *z* = 5 mm. The cross indicates the tumour site.

Figure 12. Relative permittivity displayed on the *xy* plane cutting the model at *z* = 5 mm. The cross indicates the tumour site.

However, we are quite confident that the performed optimization could be improved by optimizing not only the phases of the array elements, but also their relative amplitudes.

5. Interpolated neck model

Finally, we briefly introduce our attempts to reproduce the neck segmentation using the freeware Zubal phantom data [7]. For our analyses, we downloaded the original head/body torso phantom with no arms or legs attached, generated from the segmentation of the CT scan of a human male and re-arranged to create a 128×128×243 byte volume with isotropic voxel dimensions of 4 mm. Each voxel of the volume contains an index number designating it as belonging to a given organ or internal structure.

Starting from this data set, we have first identified the slices corresponding to the neck region (from #40 to #62), reducing the data matrix dimensions to 128×128×23. Then, following the approach described in [6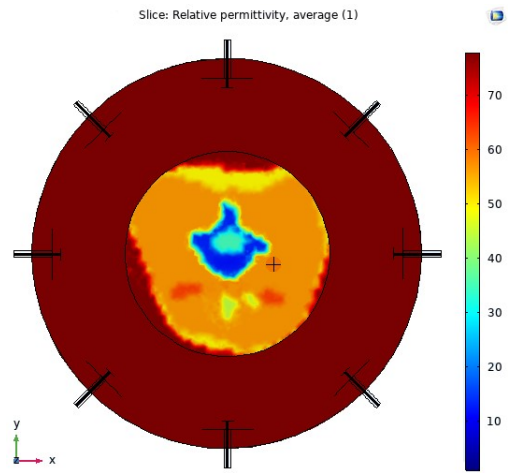], we created a text file with material data in the Spreadsheet format, where the first three columns contain the *x*, *y*, and *z* coordinates, and the following columns the corresponding values of all the considered material properties (one for each column).

To the points located outside the neck region (corresponding to the Zubal index number 0) we associated the material properties of the demineralized water, to create a continuity between the neck region and the waterbolus.

Then, we generated a cylinder in the COMSOL Multiphysics model, with a little sphere inside (the tumour). We defined how many Interpolation Functions (in the Global Definitions section) as the number of considered material properties, specifying the arguments and function units, as well as the "Position in file" number (which corresponds to the number of the associated property column in the imported text file, starting from 1). Then, in the Materials section, we associated a Blank Material node to the neck cylinder (excluding the tumour sphere), introducing in the property fields the names of the corresponding interpolation functions. The tumour properties are instead assigned to the tumour spherical region, as in the previously described examples.

Figures 10-12 show the resulting dielectric properties maps evaluated in post-processing on the model's domain. As can be observed, the material properties correctly vary according to the Zubal tissue segmentation. As suggested in [6], additional strategies could be adopted to refine the mesh along the shape of the neck (or even in the complete domain) to better resolve the transitions among the different tissues.

A SAR-based optimization was performed again using this model, following the same procedure described in the previous sections.
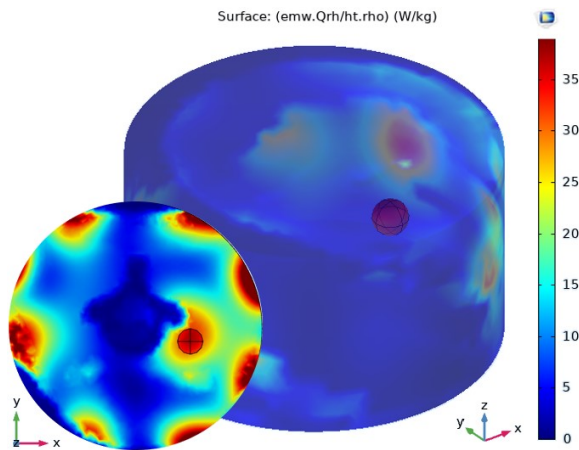
Figure 13. Surface visualization of the SAR distribution in the interpolated neck region. The inset shows the SAR on the xy plane cutting the tumour at $z = 0$.

Fig. 13 reports the 3D surface visualization of the SAR distribution, obtained after 265 iterations of the PSO, using both the phases φ_n and the amplitudes v_n as input variables. No acceptable results are indeed obtained in this case using only the phases.

As can be noted, the SAR seems to be correctly focused on the tumour region; however, different energy spots on the neck skin are revealed.

6. Conclusions

Models of the human anatomy serve an important role for many computer-based modeling and simulation calculations. In particular, in this paper, we have shown different strategies that can be adopted in COMSOL Multiphysics to reproduce a segmented phantom of the human neck.

Using LiveLink for MATLAB, we implemented a SAR-based optimization, aimed at focusing the field radiated by a proper applicator on a target region inside the neck (the tumour).

The achieved results show a robust SAR optimization which only involves the antenna phases for the basic (unrealistic) neck phantom, modeled with simple geometric elements (cylinders and spheres). When the simple neck model is replaced by more complex phantoms (the realistic VHP model as well as the Zubal phantom), a sufficiently good focusing requires the optimization of both the phases and the amplitudes of the antennas and therefore longer computational times.

Finally, it should be noted that all the presented modeling approaches could be applied to any other portion of the human body.

7. References

[1] N. R. Datta et al., "Local hyperthermia combined with radiotherapy and-/or chemotherapy: Recent advances and promises for the future", *Cancer Treat. Rev.*, vol. 41, pp. 742-753, 2015.

[2] M. W. Dewhirst et al., *Holland-Frei Cancer Medicine*, Chapter 41: *Hyperthermia*, 6th ed., B. C. Decker, 2003.

[3] M. M. Paulides et al., "The HYPERcollar: A novel applicator for hyperthermia in the head and neck", *Int. J. Hyperthermia*, vol. 23, no. 7, pp. 567-576, 2007.

[4] M. M. Paulides et al., "A Patch Antenna Design for Application in a Phased-Array Head and Neck Hyperthermia Applicator", *IEEE Trans. Biomed. Eng.*, vol, 54, no. 11, pp. 2057-63, 2007.

[5] S. N. Makarov et al., "Virtual Human Models for Electromagnetic Studies and Their Applications", *IEEE Rev. Biomed. Eng.*, vol. 10, pp. 95-121, 2017.

[6] H. Gothäll, "Interpolating Material Data on a Regular Shape as an Alternative to Building an Irregular Geometry", COMSOL Application ID: 59131.

[7] I. G. Zubal et al., "Computerized three-dimensional segmented human anatomy", *Med. Phys.*, vol. 21, n. 2, pp. 299-302, 1994.

[8] P. Hasgall, IT'IS database for thermal and electromagnetic parameters of biological tissues. Version 4.0, 2018.

[9] R. F. Verhaart et al., "Accurate 3D temperature dosimetry during hyperthermia therapy by combining invasive measurements and patient-specific simulations", *Int. J. Hyperthermia*, vol. 31, no. 6, pp. 686-92, 2015.

[10] R. A. M. Canters et al., "Patient positioning in deep hyperthermia: influences of inaccuracies, signal correction possibilities and optimization potential", Phys. *Med. Biol*, vol. 54, no. 12, pp. 3923-36, 2009.

[11] "From Surface Mesh to Geometry: STL Import of a Vertebra", COMSOL Application ID: 30951.

8. Acknowledgments